Spike Firing Pattern of Output Neurons of the *Limulus* Circadian Clock

Jiahui S. Liu and Christopher L. Passaglia

J Biol Rhythms 2011 26: 335
DOI: 10.1177/0748730411409712

Spike Firing Pattern of Output Neurons of the *Limulus* Circadian Clock

Jiahui S. Liu and Christopher L. Passaglia[1]
Department of Biomedical Engineering, Boston University, Boston, MA

Abstract The lateral eyes of the horseshoe crab (*Limulus polyphemus*) show a daily rhythm in visual sensitivity that is mediated by efferent nerve signals from a circadian clock in the crab's brain. How these signals communicate circadian messages is not known for this or other animals. Here the authors describe in quantitative detail the spike firing pattern of clock output neurons in living horseshoe crabs and discuss its possible significance to clock organization and function. Efferent fiber spike trains were recorded extracellularly for several hours to days, and in some cases, the electroretinogram was simultaneously acquired to monitor eye sensitivity. Statistical features of single- and multifiber recordings were characterized via interval distribution, serial correlation, and power spectral analysis. The authors report that efferent feedback to the eyes has several scales of temporal structure, consisting of multicellular bursts of spikes that group into clusters and packets of clusters that repeat throughout the night and disappear during the day. Except near dusk and dawn, the bursts occur every 1 to 2 sec in clusters of 10 to 30 bursts separated by a minute or two of silence. Within a burst, each output neuron typically fires a single spike with a preferred order, and intervals between bursts and clusters are positively correlated in length. The authors also report that efferent activity is strongly modulated by light at night and that just a brief flash has lasting impact on clock output. The multilayered firing pattern is likely important for driving circadian rhythms in the eye and other target organs.

Key words in vivo recording, invertebrate, horseshoe crab, electroretinogram, circadian, efferent spike trains

Animals exhibit daily rhythms in behavioral and physiological activity due to an internal biological clock that maintains synchrony with the outside world by resetting its phase each day according to visual signals it receives from the eyes. In a diversity of animals, including humans, the clock also sends circadian signals back to visual neurons, which modulate their sensitivity to light (Jacklet, 1969; Arechiga and Wiersma, 1969; Rosenwasser et al., 1979; Barattini et al., 1981; Brandenburg et al., 1983; Bassi and Powers, 1986; Barlow, 1990). The mechanism of sensitivity modulation is complex in mammals, as multiple oscillators have been identified along the visual pathway (Dibner et al., 2010) in addition to a master clock in the suprachiasmatic nucleus (SCN). By contrast, the circadian system of horseshoe crabs is fairly simple and well understood.

The horseshoe crab clock modulates visual sensitivity directly via neural feedback to the eyes. The feedback derives from a group of cells in the cheliceral ganglia of the brain that send axon collaterals down the optic

1. To whom all correspondence should be addressed: Christopher L. Passaglia, Department of Biomedical Engineering, Boston University, 44 Cummington St., Boston, MA 02215; e-mail: psagls@bu.edu.

JOURNAL OF BIOLOGICAL RHYTHMS, Vol. 26 No. 4, August 2011 335-344
DOI: 10.1177/0748730411409712

nerves (Calman and Battelle, 1991). The efferent discharges of these cells drive anatomical and physiological changes in the eye that lower noise, increase gain, and prolong responses at night (Barlow et al., 1985), allowing the animal to see crab-like objects in moonlight and sunlight almost equally well (Powers et al., 1991). Without efferent feedback, the sensitivity rhythm is abolished, and the eyes remain in the daytime state (Barlow et al., 1977). The simple organization makes it attractive for studying clock regulation of neural function.

An unresolved question in circadian research is how clocks encode messages. While it is known that the mean spike rate of clock neurons varies diurnally (Inouye and Kawamura, 1979; Barlow, 1983; Jagota et al., 2000), presumably due to molecular feedback loops that rhythmically alter their gene expression, mean rate changes alone might not communicate the entire message. Recordings from SCN explants show that the maintained activity of clock neurons is irregular and punctuated by intermittent spike bursts (Gillette, 1991; Pennartz et al., 1998). The stochastic structure can be described by a fractal point process to a first approximation (Kim et al., 2005), suggesting that rate fluctuations on the scale of seconds to minutes may be meaningful. Such fine temporal structure has also been noted in the output of the horseshoe crab clock (Barlow, 1983), and we describe it here in experimental and quantitative detail with the goal of elucidating its relevance to clock operation or modulatory function. We show that efferent spike trains of the crab's clock in living animals are intricately constructed, with activity organized into repeating clusters of multicellular spike bursts separated by long silent periods. We suggest that the multiscale organization may be important for maintaining the target organ in the nighttime state.

MATERIALS AND METHODS

Male horseshoe crabs (*Limulus polyphemus*, 20-25 cm across carapace) were purchased from the Marine Biological Laboratory (Woods Hole, MA) or Gulf Specimen Marine Laboratory (Panacea, FL) and kept under a 12-h/12-h light-dark cycle at 20 °C in artificial seawater. After a week of acclimation to the lighting regimen, the crab was chilled in ice slurry for 10 min during its subjective morning and secured to a wooden platform with stainless steel screws. Under room light, both lateral eyes were fitted with electroretinogram (ERG) electrodes and an optic nerve recording chamber. The animal was then submerged in a tank and placed in a light-tight cage while ERGs were periodically acquired from both eyes. When ERG amplitude started increasing at subjective dusk, the lateral and median eyes were covered and efferent fiber recordings were established under focal illumination. The animal was then returned to constant darkness and data collection initiated ~15 min later. The procedures were approved by the Institutional Animal Care and Use Committee at Boston University and are described elsewhere (Liu and Passaglia, 2009).

Electroretinogram Recording

ERGs were recorded with a custom-made opaque chamber that held a saline reservoir in contact with the cornea. A silver-chloride wire in the saline conducted light-evoked signals out to a bioamplifier (XCell 3+, FHC, Inc., Bowdoinham, ME). Every 5 or 10 min, light flashes (6 kcd/m^2, 0.1 sec) were delivered to the eye in darkness by an ultra-bright LED (Model 33C1292; Newark, Inc., Chicago, IL) mounted in the chamber lid. Evoked signals were amplified, lowpass filtered at 100 Hz, and sampled at 1 kHz using custom software written in Labview (National Instruments, Austin, TX). ERG waveforms were stored and peak-to-peak amplitude was plotted versus time of day.

Efferent Nerve Recording

Efferent optic nerve activity was recorded using a suction electrode and custom chamber. The cylindrical chamber was mounted by cutting a hole of the same diameter in the carapace and securing with screws. After clearing overlying tissue, the nerve was gently pulled with thread into the chamber through a slot at the bottom. The slot was then padded with cotton, and the chamber was filled with Ringer's solution. At nightfall, the nerve was visualized with a stereoscope (SMZ-168; Jed Pella, Inc., Redding, CA) and a tiny fiber was cut free. The end from the brain was guided into the tip of the Ringer-filled suction electrode (A-M Systems, Inc., Sequim, WA). If the fiber was active, the recorded signal was amplified, filtered, and continuously digitized at 8 kHz to computer until activity was lost. Times of spike firing were extracted by a custom-written MATLAB program (The MathWorks, Inc., Natick, MA) that used signal-to-noise ratio and peak-to-trough times to identify action potentials. Spike waveforms were often similar in shape and computationally difficult to sort, so they were combined into a single train of events. Based on smaller data sets of manually

identified spikes, the program identified >99% of all events in a typical recording.

Serial Correlation Analysis

Temporal patterning of spikes was assessed by serial correlation analysis. Records were divided into segments of 500 to 3000 interspike intervals (ISIs), depending on record length, and the serial correlation s_k between one ISI τ_i and another k-intervals later, τ_{i+k} was computed as

$$s_k = \frac{N\sum_{i=1}^{N}\tau_i\tau_{i+k} - \sum_{i=1}^{N}\tau_i\sum_{i=1}^{N}\tau_{i+k}}{\sqrt{\left[N\sum_{i=1}^{N}\tau_i^2 - \left(\sum_{i=1}^{N}\tau_i\right)^2\right]\left[N\sum_{i=1}^{N}\tau_{i+k}^2 - \left(\sum_{i=1}^{N}\tau_{i+k}\right)^2\right]}} - \frac{k-N}{N(N-1)},$$

where N is the number of ISIs per segment. The second term is a correction factor so that the expected value of s_k is zero when no correlation exists (Goldberg et al., 1964). For a given lag k, the correlation coefficient is positive if the pair of intervals both tend to be short or long, and it is negative if one tends to be short and the other long.

Power Spectral Analysis

Temporal patterning of spikes was further assessed by power spectral analysis. Records were divided into segments of 600 sec, and for each segment, a discrete-time sequence was formed by counting spikes in successive 0.1-sec bins. The power spectrum was then calculated by squaring the discrete Fourier transform of each sequence and averaging across sequences to obtain mean power spectral densities. The segmenting procedure reduced noise in the density estimates at the cost of spectral resolution. The bin size was selected after initial analyses with smaller bins did not reveal additional spectral features in single-fiber spike trains.

RESULTS

Data were collected from 19 horseshoe crabs beginning after subjective dusk when clock efferent neurons are active. Efferent firing patterns were similar across data sets, and those lasting until subjective dawn were quantitatively analyzed (n = 14). Some recordings persisted multiple nights (n = 4), providing information about activity onset. Most data sets contained several active efferent fibers. On occasion (n = 6), a single fiber was recorded.

Multilayered Organization of Efferent Spike Trains

As reported previously (Barlow et al., 1977; Barlow, 1983), the horseshoe crab eye shows a diurnal rhythm in visual sensitivity that is driven by the spike discharges of efferent optic nerve fibers of the circadian clock (Fig. 1A). Clock output neurons are silent during the day, ramp on at dusk (zeitgeber time: ZT12) to a maintained rate of ~1 impulse/sec (ips) per efferent fiber, and wind off at dawn (ZT0). Although the clock's influence on visual sensitivity spans several hours, efferent spike trains exhibit surprisingly rich structure at fast time scales (Fig. 1B). On a scale of milliseconds, action potentials are fired in near-synchronous multicellular bursts (bottom). The burst duration depends on the number of recorded fibers but lasts no longer than 0.2 to 0.3 sec. On a scale of seconds, the spike bursts then repeat at semi-regular intervals to form clusters of varying length and burst number (middle). For most animals, the clusters of spike bursts are separated by long intervals of quiescence (top). On a scale of minutes, the silent periods organize clock output into packets of clusters of bursts.

The progression of efferent firing patterns across the night was examined by plotting the time interval between successive spikes (ISI). For dual- and multifiber data sets, 3 bands can be identified in the scatter plots: a dense short band (ISIs <0.2 sec) from spikes in a burst, a medium band (ISIs ~1-5 sec) from bursts in a cluster, and a broad sparse long band (ISIs >5-10 sec) from the silent periods between clusters (Fig. 1C, left and right). Single-fiber data sets, in contrast, present 2 bands: medium and long (Fig. 1C, middle). The lack of a short ISI band indicates that clock output neurons contribute no more than 1 spike to a burst. The spike is fired at a characteristic time relative to spikes from other neurons, as evidenced by the narrow dispersion of short ISIs in dual-fiber data sets. The multiband structure builds quickly after dusk (left). From the moment of activity onset, efferent spikes occur in bursts, and over the following hour, the bursts aggregate to form distinct clusters. The structure is maintained until about an hour before dawn when clusters dissociate as burst intervals grow increasingly long and erratic (middle and right). Clock output neurons continue to fire spikes in bursts, though, until activity ceases.

Organization of Efferent Spikes within Bursts

To gain further insight into the organization of clock output, the pattern of efferent spikes within bursts was examined. Figure 2A presents a multifiber recording in

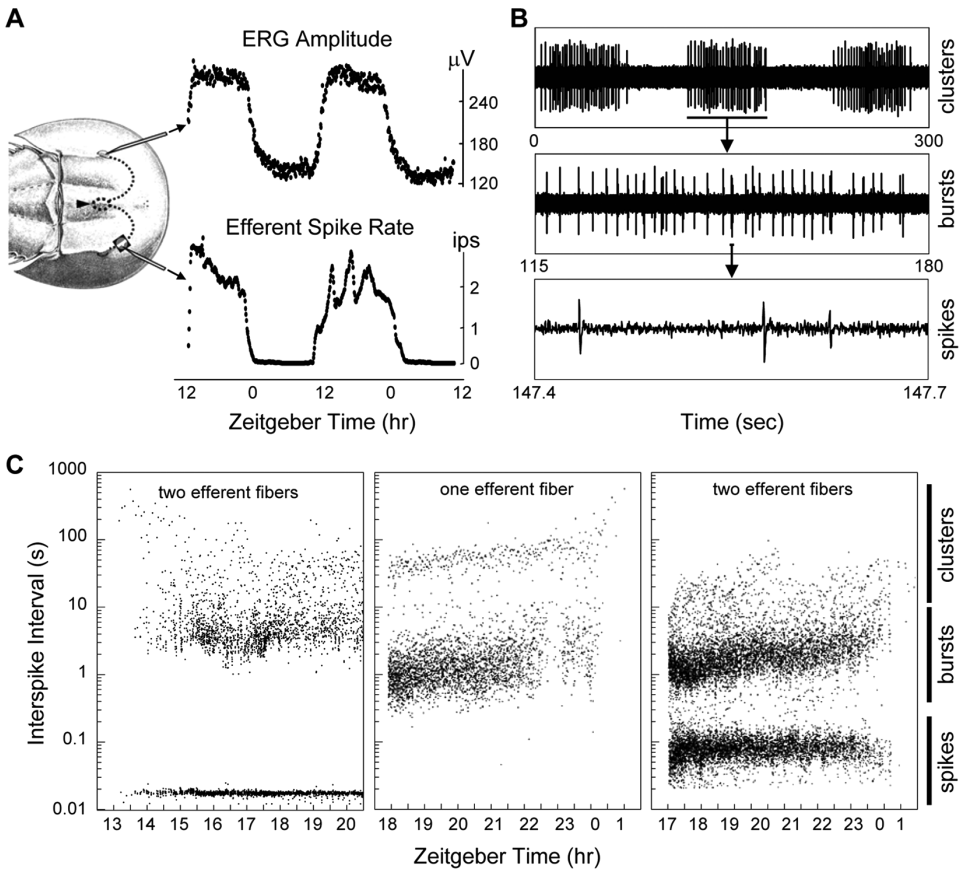

Figure 1. Temporal structure of circadian clock activity. (A) Simultaneous recording of crab electroretinogram (ERG) and efferent optic nerve spike trains. ERGs were elicited every 5 min by a brief flash in constant darkness, and the top panel plots peak-to-peak amplitude. Efferent fiber discharges were recorded in vivo from the opposite eye, and the bottom panel plots average rate (impulses per sec, ips) in 5-min intervals. Data are expressed in zeitgeber time (ZT), with ZT0 indicating when light would have turned on. The two measures are tightly correlated because the ERG reflects the summed response of photoreceptors to light and efferent spikes drive circadian changes in photoreceptor sensitivity. Dotted lines mark the optic nerves and brain (arrow). (B) Multiunit efferent recording plotted on different time scales. Clock output exhibits multilayered structure, ranging from a burst of spikes (bottom), to a cluster of spike bursts (middle), to a packet of burst clusters (top). Data set: e02. (C) Interspike interval scatterplot of efferent activity recorded in 3 experiments (e09, e07, and e08) after activity onset at dusk (left) and until activity offset at dawn (middle and right). All spikes were lumped into a single train for the dual-fiber recordings. Short, medium, and long bands are apparent corresponding to intervals between spikes, between bursts, and between clusters, respectively (bars).

which one fiber had a triphasic spike waveform (triangle) that was readily distinguishable from others. Inspection of a 5-min record confirmed that this neuron contributed a single spike to nearly every burst (101/102 bursts). Moreover, the timing of the triphasic spike was not random but rather biased to the last or second-to-last position in 97% of bursts (Fig. 2B). This could mean the fiber had the slowest conduction velocity, except that one fiber (circle) tended to fire at the beginning and two others (square) in tandem near the middle of bursts. The loose ordering of spikes implies that conduction to the recording site was not the sole cause of timing differences and that clock output neurons have a preferred firing sequence. Up to 7 spike waveforms were recorded in this experiment, and although the triphasic spike was highly reliable, not every burst presented the full set of waveforms (Fig. 2C). In some instances, this could not be explained by spike overlap because just 4 waveforms were apparent, so clock output neurons may skip a beat sometimes.

Organization of Efferent Bursts within Clusters

The burst analysis indicates that clock output neurons are functionally coupled. Not only do they fire spikes together, but they also tend to activate with a preferred order, presumably due to a common input or interconnections among the neurons. A semi-rhythmic process then drives the coupled network, imparting cluster structure onto the output. A statistical description of the clustering process was developed by examining the temporal patterning of efferent bursts. Single-fiber recordings were especially useful for the cluster analysis because strings of spikes can be treated as clusters of bursts based on the above burst analysis (Fig. 3A). Additional support for the idea is provided by the ISI distribution (Fig. 3B), which lacks short (<0.5-sec) intervals. Burst relationships were first evaluated via the joint ISI density matrix. This matrix relates the length of interval n to a subsequent interval $n + k$. For $k = 1$, the data concentrate along the diagonal for intervals <4 sec (Fig. 3C, left), indicating that adjacent burst intervals are positively correlated in length. Loosely speaking, this

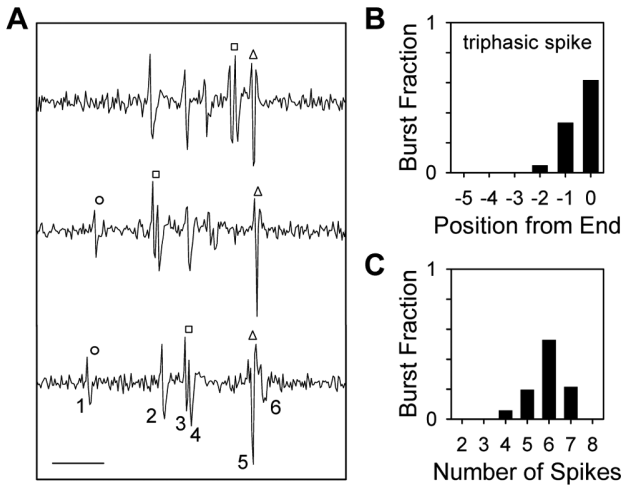

Figure 2. Organization of efferent spikes within bursts. (A) Voltage record of spike waveforms in successive bursts from a multifiber recording. The top record preceded the middle and bottom records by 2.4 and 4.9 sec, respectively. Six waveforms, numbered 1 to 6, can be identified. From inspection of 102 bursts, it was noted that the first spike (circle) in this recording often preceded the pack by ~30 msec, that two others fired in tandem (square), and that one was triphasic in shape (triangle). Bar: 20 msec. (B) Position of triphasic spike from the end of the burst. For a large fraction of bursts, the triphasic spike was last (position 0) or second to last (position –1). (C) Distribution of spike waveform count across all bursts. Data set: e11.

means that clock output neurons fire successive bursts with similar latencies. The serial correlation can be demonstrated by randomly shuffling the spike train (Fig. 3C, right). The shuffled train data scatter symmetrically around the diagonal. Other k values (<4) gave similar results (not shown), so the patterning of intervals extended beyond the next burst. Serial correlation coefficients were thereby calculated to provide a quantitative measure of burst relationships for experimental comparisons (Fig. 3D). For the example recording and database average (black symbols, left and right, $n = 12$), the coefficients are positive for short interval lags and negative for moderate lags (k = 4-11). The former is expected from Figure 3C. The latter implies that after several short interburst intervals (IBIs), there is a tendency for a long IBI and vice versa. The long IBIs correspond to the silent periods between clusters (CSIs), as evidenced by 2 data sets (e01 and e09) that showed little clustering and gave only positive coefficients (white symbols, right). The burst generation process could be closely mimicked by a stochastic leaky integrator model with IBI-dependent parameters (Suppl. Fig. S1). The IBI dependence was crucial to producing a wedge-shaped joint density matrix. It was implemented by rescaling model integration time and noise level after each burst in proportion to the actual interval length. The model did not simulate clustering, but it captured the serial correlation of burst sequences in nonclustered data sets quite well (Fig. 3D, line). Taken together, the data analysis and modeling results support the assertion that clock output is organized into clusters of bursts and that the burst generation process is semi-periodic, tending to activate at regular intervals within clusters. Model simulations suggest that this tendency arises from a stochastic interval-dependent drift in mean burst rate and a covariance of the drift noise with mean rate.

The clustering process that regulates burst generation was examined by segmenting clock output into cluster events. One complication with the segmentation procedure was the overlap in lengths of medium and long intervals, which imparted a long tail onto the ISI distribution (Fig. 3B) and muddied the distinction between the end of one cluster and the start of another. In lieu of the overlap, all intervals in the spike train exceeding a criterion length that were preceded and followed by shorter intervals were deemed CSIs, and the remainder were considered IBIs. In the case of multifiber recordings, intervals were specified by either the first spike or the largest spike in a burst. The criterion length was defined as the point at which a linear extrapolation of the cumulative ISI distribution from long to short lengths departed from the measured distribution. This definition gave reasonable estimates of burst and cluster counts based on visual inspection. For the example recording in Figure 3, nearly 95% of all bursts occurred within clusters separated by CSIs >4 sec. The burst count per cluster was broadly distributed about a median of 19, with more than half containing 10 to 30 bursts (Fig. 4A, left). Since the typical IBI lasted ~1.3 sec (Fig. 3B), cluster duration was broadly distributed about a median of 25 sec, with more than half between 16 and 43 sec (Fig. 4B, left). Nearly all clusters (>95%) ended within a minute. The fraction of time spent in burst mode was expressed as a duty cycle (DC = 1 – CSI/ICI), where ICI is the interval between the start of adjacent clusters (intercluster interval). The median DC of the recording was 0.77 (Fig. 4C, left), meaning that cluster duration was 3-fold longer than the CSI. These results are representative of the majority of recordings (Fig. 4A-C, right), except for the 2 nonclustered data sets. Burst count and cluster duration varied widely, and DC hovered near 1 in those recordings for unknown reasons. To further distill the results, data sets that exhibited clustering were combined (line). The

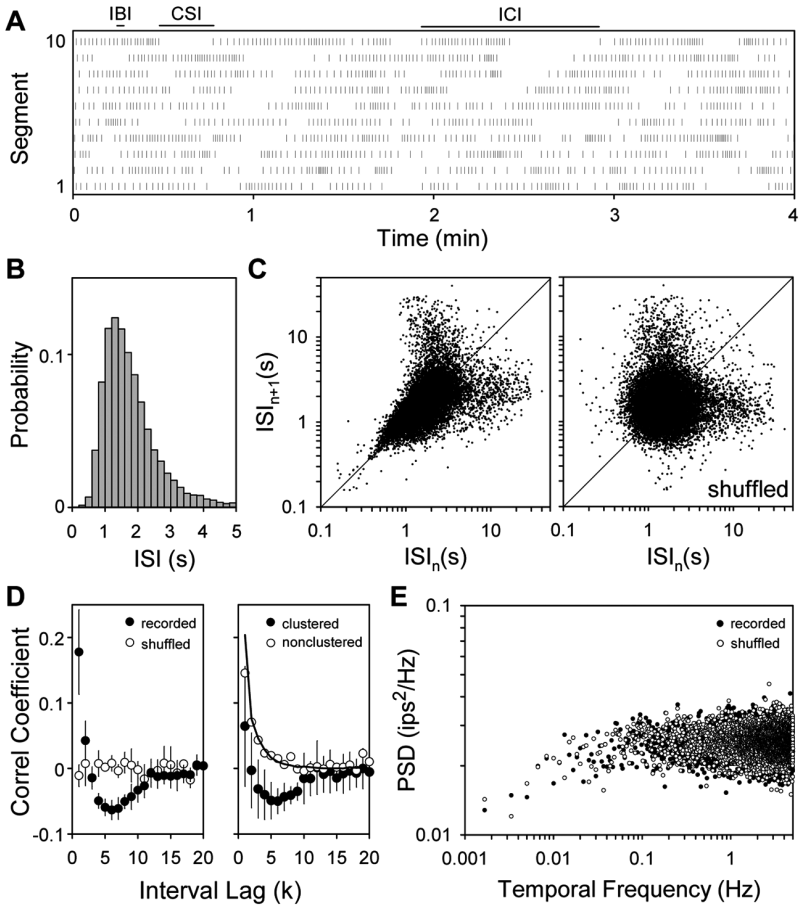

Figure 3. Organization of efferent bursts and burst clusters. (A) Raster plot of the spike train of a single efferent fiber recorded from 1800-1840 ZT in 4-min segments. Data set: e10. Each mark identifies a spike fired by the fiber and represents a burst of efferent activity based on Figure 2. A grouping of spikes thereby corresponds to a cluster of bursts. IBI, CSI, and ICI are the times between the start of sequential bursts (interburst interval), between sequential clusters (cluster silent interval), and between the start of sequential clusters (intercluster interval), respectively. For this single-fiber recording, IBI is the same as ISI. (B) Relative frequency of ISIs during the middle of night when efferent firing patterns are fairly stable (1630-2230 ZT, 13,612 intervals). (C) Joint density matrix of sequential intervals (ISI_n and ISI_{n+1}). The data concentrate on the matrix diagonal (left), indicating that adjacent burst intervals tend to have similar length. This tendency is eliminated by randomly shuffling the sequence of recorded intervals (right). For intervals >4 sec, the data in both cases form horizontal and vertical bands due to CSIs. (D) Serial correlation coefficients between pairs of intervals separated by varying numbers of spikes (i.e., lags). Left plot gives the average coefficients for the single-fiber spike train before and after shuffling (black and white symbols, respectively). Right plot gives the average coefficients for 2 data sets that did not show marked clustering (e01 and e09, white symbols) and for all other data sets (black symbols). The line gives the average coefficients produced by a model of the burst generation process (see Suppl. Fig. S1). Error bars are standard deviations. (E) Power spectrum of the ICI sequence for the single-fiber spike train before and after shuffling (black and white symbols, respectively). PSD, power spectral density.

peak of the ensemble IBI distribution ranged from 0.8 to 2.6 sec about a mean of 1.6 sec. The burst count and cluster duration distributions echoed that of the example single-fiber recording, but the DC distribution did not. It had an additional mode around 0.25 due to a handful of recordings that presented a long and regular CSI by comparison (e.g., Fig. 1C).

Organization of Efferent Clusters

The cluster analysis describes the organization of intervals within and between clusters of bursts. To address the organization of clock output into packets of burst clusters and potentially higher level structures, the patterning of cluster intervals was examined. For the packet analysis, cluster events were defined as above, and the sequence of ICIs was extracted from efferent spike trains. This interval sequence marked the times between the first burst in successive clusters, and Figure 3E plots its power spectrum for the example single-fiber recording (black symbols). The spectrum is roughly sigmoidal in shape, suggesting that ICIs are gamma distributed in length and random in order (Passaglia and Troy, 2004). Consistent with this suggestion, the power spectrum is unchanged after shuffling the ICI sequence (white symbols). Other clustered data sets showed the same result, which indicates that the cluster generation process is purely stochastic and that there is no additional structure to efferent spike trains.

Light-Evoked Response of Efferent Fibers

In the process of tracking circadian modulation of eye sensitivity, it was noted that light strongly excites clock output neurons. Figure 5A plots the spike train of a single efferent fiber at night in 10-min segments. In the experiment, a brief (50-msec) flash was delivered to the lateral eyes at the 2-min mark of each segment to elicit an ERG. The fiber repeatedly responded to the flash with a short barrage of spikes followed by a prolonged period of silence. The response delay ranged from 0.2 to 2.1 sec across stimulus presentations, about an average of 0.8 sec. The large variability reflects the interaction of light input with the ongoing burst output of the clock.

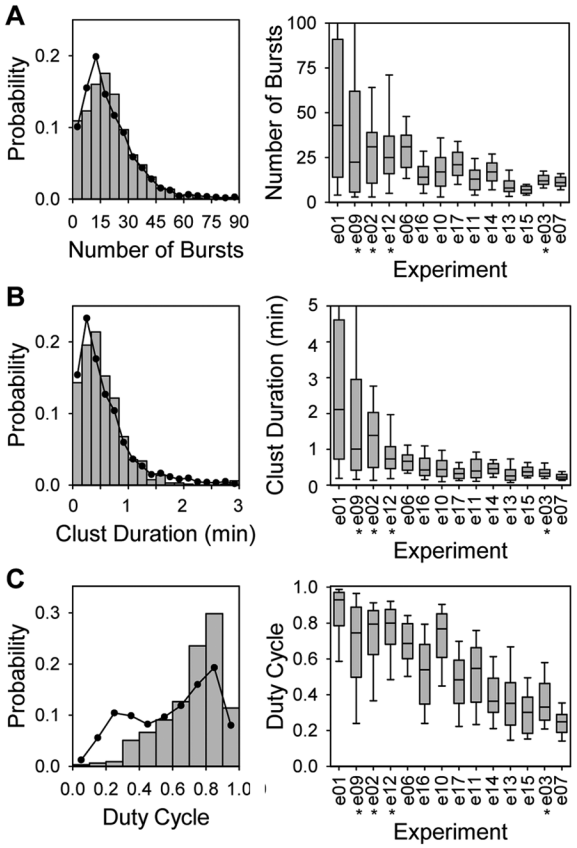

Figure 4. Efferent burst and cluster statistics. (A-C) Distribution of the total number of bursts in a cluster, the total duration of a cluster, and the ratio of cluster duration to ICI (or duty cycle). Left plots present data for the single-fiber recording of Figure 3 (bars) and all recordings that exhibited cluster structure (symbols), which excluded e01 and e09. Right plots give summary data for each experiment, where the box marks the median, upper, and lower quartiles and the whiskers mark the 5th and 95th percentiles. Only the first night is shown for multinight experiments (asterisks).

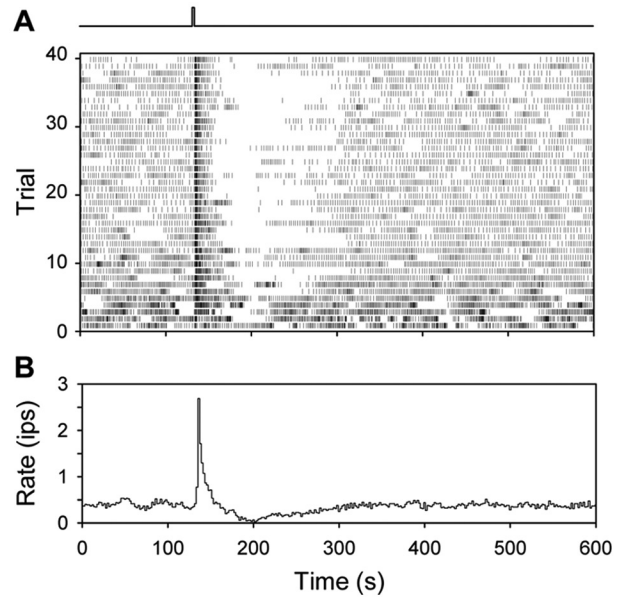

Figure 5. Efferent response of the clock to light. (A) Raster plot of the spike train recorded from a single efferent fiber during which 50-ms flashes of light were delivered to both lateral eyes every 10 min. The record is presented in 10-min segments so that flash responses align in time across stimulus trials. Data set: e04. (B) Average time-varying firing rate of the efferent fiber for 40 light flashes. The durations of the transient light response and subsequent response suppression were estimated from the times at which the rate crossed and returned to the baseline level of 0.4 ips, respectively. Bin size: 2 sec.

The flash response strengthened over time due perhaps to fading of light exposure effects during fiber isolation, circadian changes in clock sensitivity to light at night, or adaptation of clock neurons to repeated stimulation. The rate increase and subsequent decrease lasted approximately 18 sec and 160 sec (Fig. 5B), respectively, which is much too slow for afferent optic nerve fibers and clearly must derive from the brain. Indeed, stimulation of any eye evoked a light response. In every case (n = 3), the response could only be elicited during subjective night.

DISCUSSION

The efferent output of the *Limulus* circadian clock has a complex temporal structure. Clock output neurons fire spikes in near-synchronous bursts, with each neuron contributing 1 spike to virtually every burst. The timing of their spikes within a burst is variable but follows a preferred order. The neurons fire synchronously from the moment of activity onset at dusk until activity offset at dawn. The interburst interval is typically around 1 to 2 sec and covaries in length with nearby bursts. Shortly after dusk, the spike bursts group in time to form clusters that are separated by longer intervals of silence. The number of bursts per cluster and cluster duration can vary widely, but more than half of the clusters contain between 10 and 30 bursts and last from 16 to 43 sec. The silent period between clusters is also variable in length for most animals and can range from several seconds to over a minute. The burst generation process has interval memory, which correlates clock output within clusters. In contrast, the cluster generation process refreshes after each silent period so the sequence of cluster start times is effectively random. Clock neurons also respond to light at night. Light is disruptive to their endogenous activity rhythm, abolishing efferent spikes for minutes after just a brief flash. It is likely that clock firing

patterns have functional relevance in view of their complex structure, and this study provides the first quantitative description of the structure in living animals. The findings give insight into the organization of the *Limulus* clock and perhaps into how all circadian clocks drive physiological changes with neural messages.

Relation to Clock Firing Patterns in Mammals

Like horseshoe crabs, circadian clock neurons in mammals are periodically active, and the variation in mean firing rate over the day-night cycle is considered an important element of clock function. One noticeable difference is that clock output is high during the day and low at night (Inouye and Kawamura, 1979; Gillette, 1991). Recordings from individual SCN neurons show a diversity of firing patterns. Most cells discharge sporadically at irregular rates or intermittently in bursts, whereas others fire in regular intervals (Groos and Hendriks, 1979; Pennartz et al., 1998; Schaap et al., 2003; Jeong et al., 2005). The coefficient of variation (CV) of ISIs is <0.3 for regular cells, similar to pacemaker neurons, while CV ranges from 0.3 to 0.8 for irregular and burst cells. It was suggested that burst cells might drive or modulate SCN excitability because they have low spontaneous activity and an extensive network of local axon collaterals. The function of the other types is unknown. The firing pattern of *Limulus* clock neurons most resembles that of irregular or burst cells, but it is considerably more variable (CV = 1-3) due to the tendency of bursts to cluster together. The resemblance is striking, though, if CSIs are removed from their spike train or nonclustered data sets are considered (CV = 0.4-0.7).

Putative Relevance of Clock Firing Patterns

Efferent optic nerve fibers originate from two groups of ~15 cells located in the cheliceral ganglia on opposite sides of the *Limulus* brain (Calman and Battelle, 1991). The fibers are small in diameter (0.5-2 µm) and number (0.1%-0.2%) compared to afferent nerve fibers, and they project bilaterally to the lateral eyes and several other light-sensing organs (Fahrenbach, 1971; Evans et al., 1983). We presume few were recorded in an experiment because the fibers were often found in dorsolateral bundles of the nerve that are easily damaged during surgical exposure. At present, it is not known whether cheliceral ganglion cells are central components of the circadian clock or an output pathway for modulating visual sensitivity. This raises two possible explanations for the complex structure of efferent spike trains.

One possibility is that the multiscale patterning of spikes might reflect the timekeeping mechanism of the clock network. The SCN clock in mammals is known to contain a multiphasic network of synaptically and electrically coupled cells (Quintero et al., 2003; Welsh et al., 2010). It has been proposed that a circadian period could be constructed from a hierarchical cascade of shorter period ultradian oscillators (Dowse and Ringo, 1987; Barrio et al., 1997). The passing of seconds might thereby be communicated within the *Limulus* clock network by IBIs, the passing of minutes by ICIs, and so forth. If this idea has merit, it is not apparent from the periodicity of efferent spikes, bursts, and clusters, which are fairly variable and present only at night. Moreover, SCN cells express molecular rhythms with a 24-h period (Ko and Takahashi, 2006), implying that the timekeeping mechanism of the clock is subcellular.

A more likely possibility is that the temporal patterning of efferent spikes is important for transmitting circadian messages to target organs. It is known that stimulation of efferent fibers at 2 Hz can mimic endogenous clock-driven changes in visual sensitivity (Barlow, 1983) and that the mechanism of action is octopamine, which increases cAMP levels in photoreceptor cells and pushes the retina into its nighttime state (Battelle, 2002). The ultrastructure of efferent synapses suggests that octopamine release involves a neurosecretory process (Kass and Barlow, 1984), and a common feature of neurosecretory cells in many species is burst activity (van Swigchem, 1979; Brown et al., 1998; Brierley et al., 2001). Moreover, burst and burst clusters have been shown to enhance neuropeptide release even if the mean firing rate is kept constant (Dutton and Dyball, 1979). The burst and cluster activity of efferent nerve fibers in horseshoe crabs might therefore be structured to maintain or potentiate octopamine effects on the eye, and silent periods between clusters may be needed for transmitter reuptake or recovery. A caveat to this idea is that efferent bursts reflect the discharges of several fibers. An individual clock output neuron does not fire in rapid succession like typical neurosecretory cells.

The strength of the horseshoe crab model for circadian research is that these possibilities can be directly evaluated by electrically stimulating the optic nerve with different patterns and monitoring ERG changes. This study provides a detailed description of clock firing patterns and quantitative information about major pattern features, which can be used to realistically simulate or systematically manipulate the clock's input to the eye.

ACKNOWLEDGMENTS

The work was supported by NSF CAREER Award BES-0547457. We thank Nadav Ivzan for technical assistance.

CONFLICT OF INTEREST STATEMENT

The author(s) have no potential conflicts of interest with respect to the research, authorship, and/or publication of this article.

NOTE

Supplementary material for this article is available on the *Journal of Biological Rhythms* website at http://jbr.sagepub.com/supplemental.

REFERENCES

Arechiga H and Wiersma CAG (1969) Circadian rhythm of responsiveness in crayfish visual units. J Neurobiol 1:71-85.

Barattini S, Battisti B, Cervetto L, and Marroni P (1981) Diurnal changes in the pigeon electroretinogram. Rev Can Biol 40:133-137.

Barlow RB (1983) Circadian rhythms in the *Limulus* visual system. J Neurosci 3:856-870.

Barlow RB (1990) What the brain tells the eye. Sci Am 262:90-95.

Barlow RB, Bolanowski SJ, and Brachman ML (1977) Efferent optic nerve fibers mediate circadian rhythms in the *Limulus* eye. Science 197:86-89.

Barlow RB, Kaplan E, Renninger GH, and Saito T (1985) Efferent control of circadian rhythms in the *Limulus* lateral eye. Neurosci Res 2(Suppl):S65-S78.

Barrio RA, Zhang L, and Maini PK (1997) Hierarchically coupled ultradian oscillators generating robust circadian rhythms. Bull Math Biol 59:517-532.

Bassi CJ and Powers MK (1986) Daily fluctuations in the detectability of dim lights by humans. Physiol Behav 38:871-877.

Battelle B (2002) Circadian efferent input to *Limulus* eyes: Anatomy, circuitry, and impact. Microsc Res Tech 58: 345-355.

Brandenburg J, Bobbert AC, and Eggelmeyer F (1983) Circadian changes in the response of the rabbit's retina to flashes. Behav Brain Res 7:113-123.

Brierley MJ, Ashworth AJ, Banks JR, Balment RJ, and McCrohan CR (2001) Bursting properties of caudal neurosecretory cells in the flounder *Platichthys flesus*. J Exp Biol 204:2733-2739.

Brown CH, Ludwig M, and Leng G (1998) Kappa-opioid regulation of neuronal activity in the rat supraoptic nucleus in vivo. J Neurosci 18:9480-9488.

Calman BG and Battelle B-A (1991) Central origin of the efferent neurons projecting to the eyes of *Limulus polyphemus*. Vis Neurosci 6:481-495.

Dibner C, Schibler U, and Albrecht U (2010) The mammalian circadian timing system: Organization and coordination of central and peripheral clocks. Annu Rev Physiol 72:517-549.

Dowse HB and Ringo J (1987) Further evidence that the circadian clock in *Drosophila* is a population of coupled ultradian oscillators. J Biol Rhythms 2:65-76.

Dutton A and Dyball RE (1979) Phasic firing enhances vasopressin release from the rat neurohypophysis. J Physiol 290:433-440.

Evans JA, Chamberlain SC, and Battelle B-A (1983) Autoradiographic localization of newly synthesized octopamine to retinal efferents in the *Limulus* visual system. J Comp Neurol 219:369-383.

Fahrenbach WH (1971) The morphology of the *Limulus* visual system: IV. The lateral optic nerve. Z Zellforsch 114:532-545.

Gillette MU (1991) SCN electrophysiology in vitro: Rhythmic activity and endogenous clock properties. In *Suprachiasmatic Nucleus: The Mind's Clock*, Klein DC, Moore RY, Reppert SM, eds, pp 125-143. New York: Oxford University Press.

Goldberg JM, Adrian HO, and Smith FD (1964) Response of neurons of the superior olivary complex of the cat to acoustic stimuli of long duration. J Neurophysiol 27: 706-749.

Groos GA and Hendriks J (1979) Regularly firing neurones in the rat suprachiasmatic nucleus. Experientia 35:1597-1598.

Inouye ST and Kawamura H (1979) Persistence of circadian rhythmicity in a mammalian hypothalamic island containing the suprachiasmatic nucleus. Proc Natl Acad Sci U S A 76:5962-5966.

Jacklet JW (1969) Circadian rhythm of optic nerve impulses recorded in darkness from isolated eye of *Aplysia*. Science 164:562-563.

Jagota A, de la Iglesia HO, and Schwartz WJ (2000) Morning and evening circadian oscillations in the suprachiasmatic nucleus in vitro. Nat Neurosci 3:372-376.

Jeong J, Kwak Y, Kim YI, and Lee KJ (2005) Dynamical heterogeneity of suprachiasmatic nucleus neurons based on regularity and determinism. J Comp Neurosci 19:87-98.

Kass L and Barlow RB (1984) Efferent neurotransmission of circadian rhythms in *Limulus* lateral eye: I. Octopamine-induced increases in retinal sensitivity. J Neurosci 4: 908-917.

Kim SI, Jeong J, Kwak Y, Kim YI, Jung SH, and Lee KJ (2005) Fractal stochastic modeling of spiking activity in suprachiasmatic nucleus neurons. J Comp Neurosci 19:39-51.

Ko CH and Takahashi JS (2006) Molecular components of the mammalian circadian clock. Hum Mol Genet 15:271-277.

Liu JS and Passaglia CL (2009) Using the horseshoe crab, *Limulus polyphemus*, in vision research. J Vis Exp (29):pii: 1384. doi:10.3791/1384.

Passaglia CL and Troy JB (2004) Information transmission rates of cat retinal ganglion cells. J Neurophysiol 91:1217-1229.

Pennartz CM, De Jeu MT, Geurtsen AM, Sluiter AA, and Hermes ML (1998) Electrophysiological and morphological heterogeneity of neurons in slices of rat suprachiasmatic nucleus. J Physiol 506:775-793.

Powers MK, Barlow RB, and Kass L (1991) Visual performance of horseshoe crabs day and night. Vis Neurosci 7:179-189.

Quintero JE, Kuhlman SJ, and McMahon DG (2003) The biological clock nucleus: A multiphasic oscillator network regulated by light. J Neurosci 23:8070-8076.

Rosenwasser AM, Raibert M, Terman JS, and Terman M (1979) Circadian rhythm of luminance detectability in the rat. Physiol Behav 23:17-21.

Schaap J, Pennartz CM, and Meijer JH (2003) Electrophysiology of the circadian pacemaker in mammals. Chronobiol Int 20:171-188.

van Swigchem H (1979) On the endogenous bursting properties of 'light yellow' neurosecretory cells in the freshwater snail *Lymnaea stagnalis*. J Exp Biol 80:55-67.

Welsh DK, Takahashi JS, and Kay SA (2010) Suprachiasmatic nucleus: Cell autonomy and network properties. Annu Rev Physiol 72:551-577.